Modelling higher trapped fields by pulsed field magnetisation of composite bulk MgB$_2$ superconducting rings

V Cientanni[1,*] ⓘ**, M D Ainslie**[1] ⓘ**, H Fujishiro**[2] ⓘ **and K Takahashi**[2] ⓘ

[1] Department of Engineering, University of Cambridge, Cambridge CB2 1PZ, United Kingdom
[2] Department of Physical Science and Materials Engineering, Faculty of Science and Engineering, Iwate University, Morioka 020-8551, Japan

E-mail: vc329@cam.ac.uk

CrossMark

Abstract

The recent results of Hirano *et al* (2020 *Supercond. Sci. Technol.* **33** 085002) reported a high trapped field of 1.61 T in a composite MgB$_2$ ring comprising copper plates and and a soft iron yoke magnetised by pulsed field magnetisation (PFM). Inspired by these results, an investigation using systematic modelling methods was conducted to investigate the key parameters leading to the success of Hirano *et al*. Our results indicate that composite structures of MgB$_2$ rings present a viable method of trapping high magnetic fields when magnetised with PFM. Leveraging a finite element method modelling framework with a commercial software package (COMSOL Multiphysics), we have successfully modelled the experimental data with excellent agreement. We have paid careful attention to the assumptions regarding the thermal physics, which enabled the successful and accurate modelling of the experiment. Exploiting the flexibility of computational modelling, we extend our studies to investigate the influence of the constituent elements of the composite bulk on the electromagnetic and thermal behaviour, and discuss in detail how each can enhance the trapped field performance of the bulk. Aided by the models, it is shown how the number of copper layers influences the elongation of the applied pulse, reducing the field penetration and the maximum temperature rise of the bulk. The addition of the iron yoke significantly increases the trapped field, by concentrating flux during and after the pulse.

Supplementary material for this article is available online

Keywords: bulk MgB$_2$, pulsed field magnetisation, trapped field, numerical modelling, finite element method, composite structures, soft iron yoke

(Some figures may appear in colour only in the online journal)

---

* Author to whom any correspondence should be addressed.

1. Introduction

1.1. Background

Bulk superconductors fabricated from (RE)-Ba–Cu–O (RE = rare-earth, such as Gd or Y) or MgB_2 (magnesium diboride) materials show great promise for trapping large magnetic fields, which can be exploited as permanent magnet analogues in engineering applications such as magnetic separation, superconducting rotating machines, and advanced NMR/MRI [1–4]. In 2014, a new trapped field record of 17.6 T at 26 K was achieved in a (RE)-Ba–Cu–O bulk [5], illustrating the significant application of these materials. MgB_2 bulks meanwhile, present a number of advantages over (RE)-Ba–Cu–O bulks. The lightweight, polycrystalline structure is 'rare-earth-free', can trap highly homogenous fields due to the long coherence length [6], and may be fabricated using a number of techniques with relative ease [7]. The trapped field performance of MgB_2 bulks has continued to improve with the following achievements of trapped fields in excess of 3 T; 5.6 T at 11 K with a stacked MgB_2/TiB_2 composite hot-pressed bulk [8], 5.4 T at 12 K with a single hot-pressed and milled Mg/B powder mix bulk [9], 3.75 T at 5 K with a C-doped infiltration growth bulk [10], and 3.72 T at 5 K with a ball-milled, pressure-free fabrication technique [11]. Indeed, whilst the record high trapped field of 5.6 T is lower than (RE)-Ba–Cu–O, the magnetisation potential is still great. Achieving these records involved using the field-cooled magnetisation (FCM) technique [12], which ensures full magnetisation of the bulk. This requires a large, static magnetising field from bulky and expensive magnets that are usually superconducting, so is usually reserved for sample characterisation purposes. Pulsed-field magnetisation (PFM) meanwhile has greater practical application with an inexpensive and portable setup, despite an often lower trapped field due to high thermal loading of the samples [13]. Adopting favourable magnetising coil fixtures, whilst optimising the magnetisation technique with multiple pulses and step-wise cooling, has yielded promising results for PFM [14–18]. However, thermal loads remain a constraint in achieving higher trapped fields. This in particular remains a significant challenge in MgB_2 due to a higher susceptibility to flux jumps, which results in a significant reduction in the trapped field [19]. The prevalence of this effect in MgB_2 is a result of a combination of its unique properties: short thermal transit times, highly non-linear $J_c(B, T)$ characteristics, and a low operating temperature range due to its low critical temperature, T_c, of 39 K. At lower temperatures the heat capacity reduces resulting in larger temperature fluctuations per unit of thermal energy, and thus higher likelihood of a temperature gradient to induce a flux jump.

1.2. Motivation

Hirano *et al* [20] recently trapped a record high field of 1.61 T in bulk MgB_2 magnetised by PFM, by embedding bulk MgB_2 superconducting rings between layers of copper, and inserting a soft-iron yoke. The addition of the copper inserts should increase the effective rise time of the applied pulse through the generation of eddy-currents. A longer pulse rise time reduces the heating rate on the bulk; which is thought to be beneficial to trapping higher fields when magnetising under the PFM regime [17]. Applying a pulse with a longer rise time directly by adjusting the current flowing in the magnetising coils [21, 22] is energetically less favourable, requiring bulkier and more complex equipment. The copper layers thus act passively to prolong an applied pulse. Further, their high thermal conductivity and heat capacity may be favourable in transferring heat from the bulk generated during the PFM process (however, large eddy currents may conversely heat the bulk). Meanwhile, the iron yoke inserted into the bore of the composite MgB_2 ring acts to concentrate magnetic flux during the pulse, assisting the bulk magnetisation. Therefore a large number of variables in this experiment may be controlled; from the number of copper layers and their thickness, to the presence of an iron yoke insert compared to no insert. This heeds well for numerical modelling [23, 24], where parameters such as these can be adjusted easily compared to doing so experimentally. Such flexibility was the impetus behind this work; to leverage the advantage of numerical modelling, with direct inspiration from the record breaking achievement of the experimental results reported in [20].

2. Modelling framework and assumptions

Figure 1 illustrates the geometry of the 2D axisymmetric models implemented in the FEM software package COMSOL Multiphysics version 5.4. Figure 2 meanwhile illustrates the three sample configurations modelled. The fabrication of the samples along with experimental details are outlined in Hirano *et al* [20]. The various sample configurations were all of outer diameter (OD): 60 mm, and inner diameter (ID): 20 mm and between 19 and 19.5 mm in height. An iron yoke (of diameter 20 mm and height 20 mm) can be optionally inserted into the ring bore. The 'single bulk' measured 19 mm in height, and comprised MgB_2 only. It was then sliced into two smaller annuli of 9 mm in height. Three copper annuli of 0.5 mm height were then placed between the MgB_2 slices, as per figure 2(b). The applied pulsed magnetic fields were simulated by implementing a current constraint on the 'split coil' subdomains in the model, such that the applied current density (J_{pulse}), in the 'ϕ' direction, took the form of equation (1). The value of A has units m^{-1}, and linearly increases with magnetic field from 0.46 at 1.04 T to 0.52 at 1.8 T. Constants t_s and t_d, were adjusted until the form of the current pulse matched that of the pulses applied experimentally in [20].

$$J_{pulse} = H_{ext} A \left(1 - e^{-\frac{t}{t_s}} \right) \left(e^{-\frac{t}{t_d}} \right) \quad (1)$$

The split coil PFM setup with iron yokes is described elsewhere, and has been successfully used to enhance the trapped field for both (RE)-Ba–Cu–O and MgB_2 [25–27]. The magnetic field (Hall) and temperature probes were placed to measure the central trapped field and the temperature of the sample via the sample holder, respectively. The Hall probe was located directly above the centre of the top surface of the
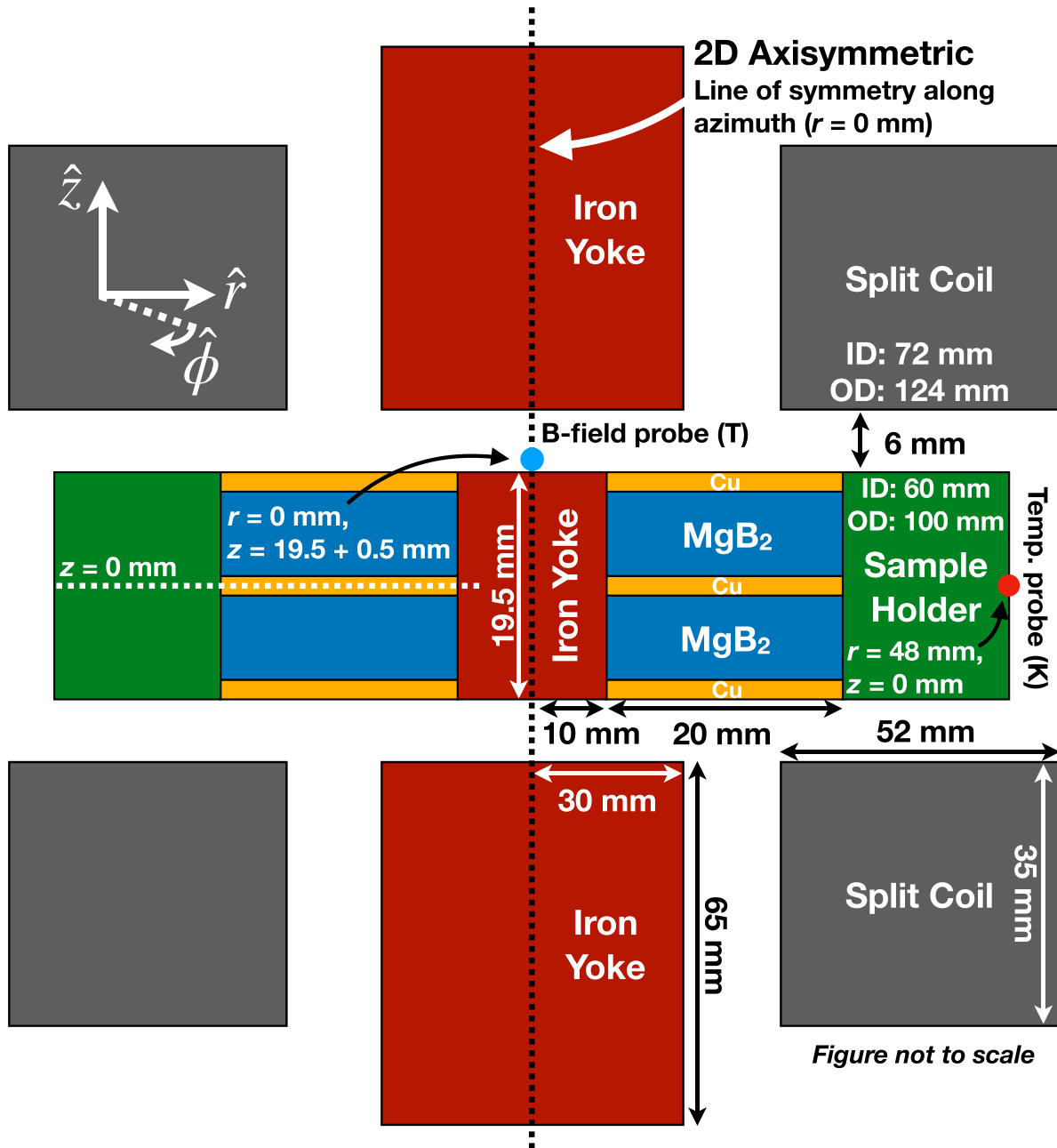
Figure 1. Geometry of the 2D axisymmetric model implemented in COMSOL Multiphysics; complete with split coil magnetisation fixture and iron yokes. The composite bulk MgB$_2$ sample is embedded in the sample holder within a vacuum space, located in the centre of the coil. The location of the magnetic field and temperature probes are labelled. The composite bulks measured 19.5 mm in height, whilst the 'single bulk' measured 19 mm.

sample ($r = 0$, $z = $ [sample height]$/2 + 0.5$ mm). The spacing of 0.5 mm in the model is to account for the active region of the Hall probe. The temperature probe meanwhile was placed radially towards the far edge of the sample holder ($r = 48$ mm, $z = 0$).

2.1. Electromagnetic considerations

The governing equations of the simulations involve coupling both electromagnetic and thermal physics. From Maxwell's equations, Faraday's law (2) and Ampere's law (3) were adopted:

$$\nabla \times \mathbf{E} = -\frac{\mathrm{d}(\mu \mathbf{H})}{\mathrm{d}t} \tag{2}$$

$$\nabla \times \mathbf{H} = \mathbf{J} \tag{3}$$

where the vector components of the magnetic field strength $\mathbf{H} = [H_z, H_r]$, the current density $\mathbf{J} = [J_\phi]$, and electric field $\mathbf{E} = [E_\phi]$. In equation (2), $\mu = \mu_o \mu_r$, where μ_o is the permeability of free space. The values of the relative permeability, μ_r, were assumed to equal 1 for all media, except the soft iron yokes for which a B–H curve was modelled following the method outlined by Ainslie *et al* [25]. The E–J power law,
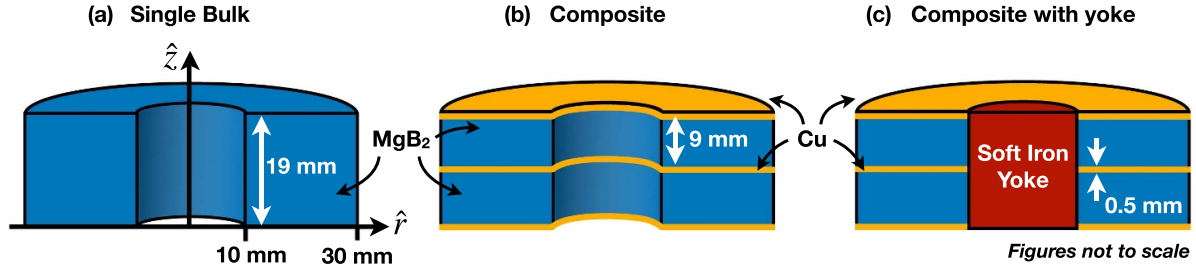
Figure 2. Configurations of the modelled composite bulk MgB$_2$ samples investigated experimentally in Hirano *et al* [20]. (a) 'single bulk' comprising only MgB$_2$, (b) 'composite without yoke' comprising MgB$_2$ sandwiched by three layers of copper and (c) 'composite with yoke' containing an inserted soft-iron yoke. The copper layer thickness is exaggerated for better visualisation. Reproduced by permission of IOP Publishing from [20].
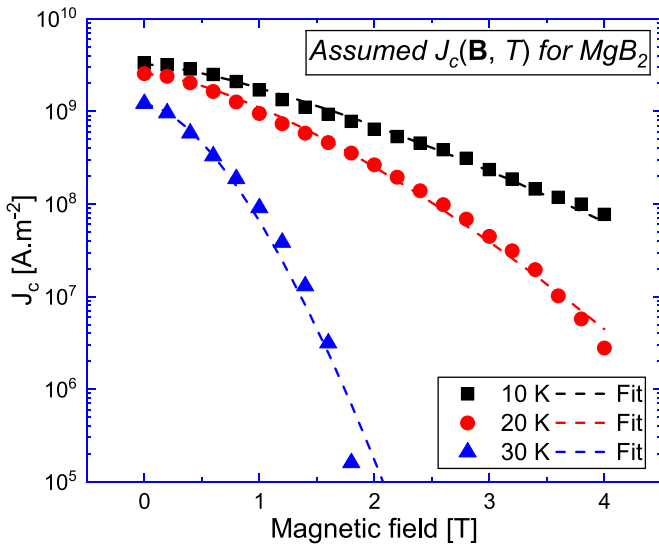

Figure 3. Assumed representative measured $J_c(B, T)$ characteristics for MgB$_2$ distribution and associated equation fits for each temperature using equation (5). Utilising these equation fits, COMSOL interpolates between them to generate a $J_c(B, T)$ surface. Reproduced by permission of IOP Publishing from [29].

represented by equation (4), was used to model the resistivity of the superconductor media; where E_o is the characteristic electric field, J_c the critical current density of the superconductor, and n the flux creep parameter. The value of n was assumed to be 45, and $E_o = 1 \times 10^{-4}$ Vm^{-1}. The J_c distribution was assumed both B and T dependent, as shown in figure 3, interpolated from data representative of the sample [28] and fit using equation (5), where α was obtained from the representative data [28], and $B_o = 0.85$ T.

$$E = E_o \left(\frac{J}{J_c} \right)^n \tag{4}$$

$$J_c(B,T) = \alpha \left(1 - \left(\frac{T}{T_c} \right)^2 \right)^{1.5} e^{-\frac{B}{B_o \left(1 - \left(\frac{T}{T_c} \right)^2 \right)^{1.5}}} \tag{5}$$

2.2. Thermal considerations

Thermal transient properties were applied exclusively to the sample and sample holder, which in the experiments were located within a vacuum space. The thermal transient equation (6) below was utilised, which permits the modelling of the conductive loss of heat via the outer radius of the sample holder r_i (thus, simulating the connection to the cold-stage). The value Q is the volumetric heating rate, equal to the product of $E_\phi \cdot J_\phi$, which provides coupling between the electromagnetic and thermal models (in addition to $J_c(B,T)$).

$$\rho c_p \frac{\partial T}{\partial t} = \kappa \nabla^2 (T_r - T_{ri}) + Q \tag{6}$$

The flow of heat to the cold stage was determined by iteratively adjusting the thermal contact conductance until the cooling rate at the temperature probe matched the data of figure 7(b) in [20]. The thermal contact conductance is thus defined as the average heat energy flowing through a boundary, divided by the temperature gradient across it. The thermal conductivity, κ, for MgB$_2$ was assumed from the data reference in table 1. All other material thermal properties were assumed isotropic, homogenous and temperature dependent; c_p, k and ρ_m, as provided in table 1. The temperature dependent electrical resistivity of each material is also given. A crucial further assumption involved controlling the thermal contact conductance between the composite bulk and the sample holder. The contact conductance between the copper layers and the sample holder was assumed a temperature independent 2.5×10^4 W m^{-2} K^{-1}. For the contact conductance between the MgB$_2$ bulk and the sample holder however, it was assumed to vary linearly between 300 W m^{-2} K^{-1} at 40 K and 1000 W m^{-2} K^{-1} at 20 K, i.e. *lower contact conductance* at higher temperatures. Whilst this may seem counterintuitive; the modelled results showed significantly better quantitative agreement, in both the time-domain and magnitude of the pulses. We justify our use of a decreasing thermal contact conductance with temperature for the interface between these two materials, by analysing their linear thermal expansion. MgB$_2$ exhibits a decreasing linear thermal expansion rate ($\Delta L/L_o$) in the temperature range modelled: 20–40 K, and is in fact even negative between 32.5 and 40 K as shown clearly by the insert

Table 1. Table of material properties.

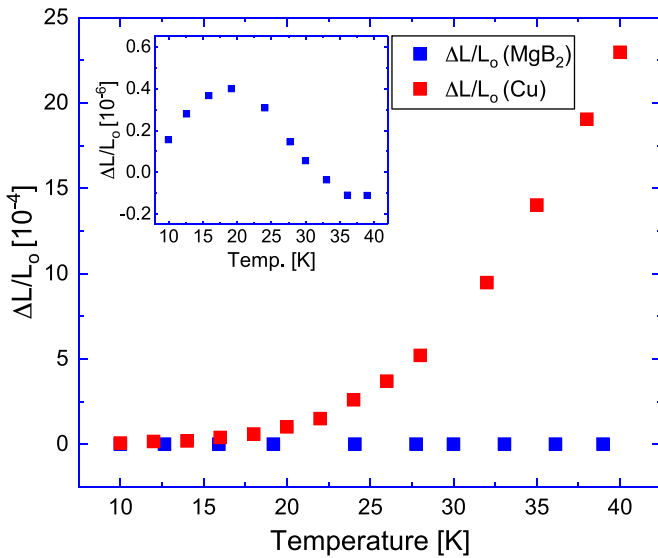| Material	Thermal conductivity ($k(T)$)	Specific heat ($c_p(T)$)	Material density (ρ_m)	Resistivity ($\rho(T)$)
MgB$_2$	[32]	[33]	2590 kg m^{-3}	$J_c(B,T)$ [28]/equation (4)
Copper			8940 kg m^{-3}	[35]
Brass	NIST [34]		8730 kg m^{-3}	$3.57 \times \rho_{Cu}$
Iron	[36]	NIST [34]	7874 kg m^{-3}	2×10^{-8} m S^{-1}

Figure 4. The increasing linear thermal expansion of Cu contrasts to the decreasing thermal expansion of MgB$_2$ between 20 and 40 K (shown with insert also) from [30] and [31]. This suggests that as both the brass sample holder and the bulk heat, the contact pressure between them reduces, reducing the effective thermal contact. Reproduced by permission of APS Publishing from [30, 31].

Figure 5. Comparison of simulation and experimental results for the trapped field of the sample under field-cooled magnetisation (FCM) from 15 K with a magnetising field of 4 T. The assumed $J_c(B,T)$ characteristics in the model are based on the interpolated data presented in figure 3.

in figure 4. Copper meanwhile is monotonically increasing in this range, and at a much larger rate. This suggests that due to the annular geometry of the sample, the brass sample holder (which we assume to behave similar to copper) may expand away from the MgB$_2$ when heated in this temperature range. This would cause a reduction in the contact pressure between the MgB$_2$ and the sample holder, and thus the effective thermal conductance should reduce in response. If this effect is indeed non-negligible, it may help explain why our use of changing the thermal layer conductance helped achieve results with better agreement between the models and experiments. Figure 4 illustrates the linear thermal expansion ($\Delta L/L_o$) of both materials; with data obtained from [30] and [31].

3. Modelling results

3.1. Pulse calibration

The success and accuracy of the models presented are a result of carefully setting up the models to replicate the experiment as closely as possible. First, to validate the assumed $J_c(B,T)$ characteristics of figure 3, the trapped field after FCM was simulated following a similar process to that described in [37],
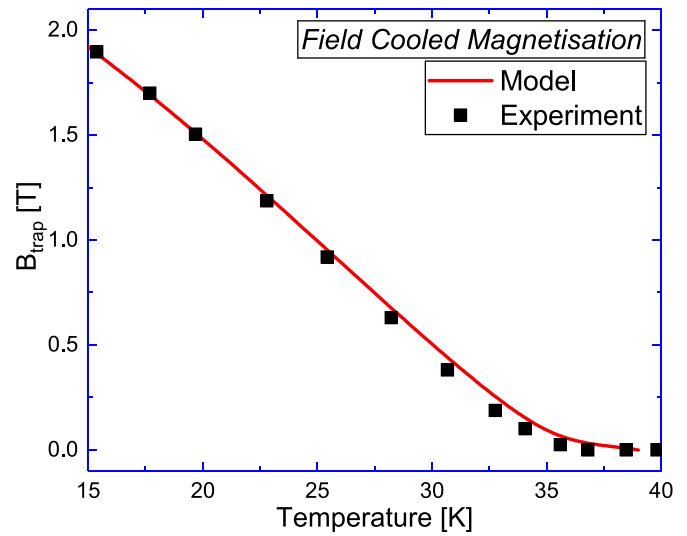
but for the 2D axisymmetric case. The composite bulk was field-cooled to 15 K with a magnetising field of 4 T, then after removing this field the temperature was gradually increased to 40 K above its T_c, observing the resulting trapped field. The results in figure 5 illustrate that the assumed $J_c(B,T)$ characteristics appropriately reproduce the expected trapped field from FCM.

The magnitude and rise time of the simulated pulse at the centre of the top surface of the sample (B(Hall)) is directly influenced by the electrical conductivity and magnetic susceptibility of the materials subject to the applied pulse (B_{app}). The rise time of the simulated pulse was matched to the experimental pulse by choosing an appropriate resistivity for the iron yoke(s) as given in table 1, whilst seeking well referenced data for the other parameters listed therein. The pulse magnitude meanwhile was calibrated using the factor A until the magnitude of the applied field B_{app} matched the peak measured value of the Hall probe B(Hall) at 40 K. Note that this follows the same experimental procedure in [20] and corresponds to the superconductor being in its normal state, $T > T_c$. The applied field B_{app} is also referred to as 'B_{ex}(shunt)' in figure 6, due to the experimentally generated pulse via a shunt resistor. It was observed that A should be linearly proportional to the applied field, whose values are given in figure 3.
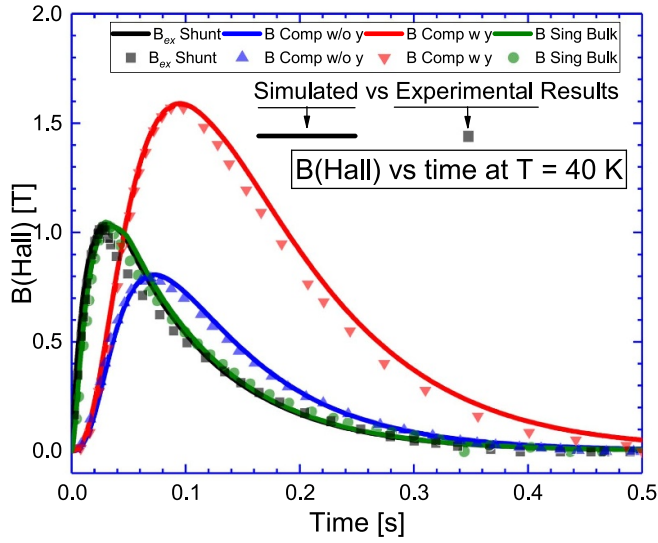
Figure 6. A comparison of the time dependence of the experimentally applied magnetic fields (scatter points) to those simulated in the model (line graphs). All data were measured (experiments; symbols) and calculated (simulations; solid lines) at the same 'Hall probe' position, 0.5 mm above the centre of the top surface of the sample at 40 K. Reproduced by permission of IOP Publishing from [20].
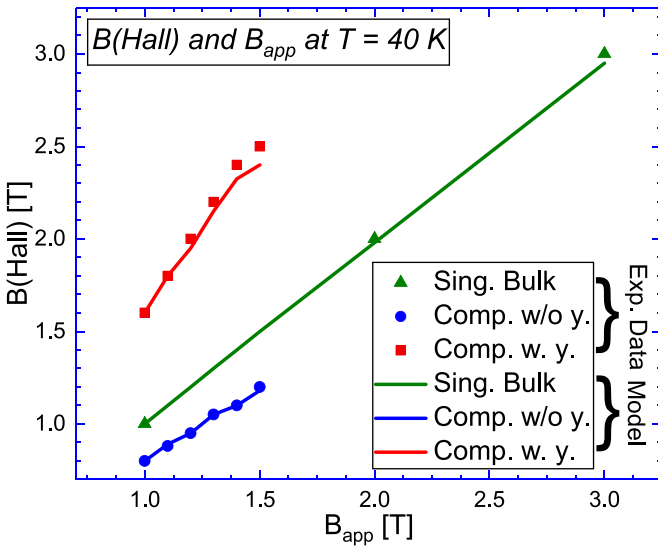

Figure 7. Applied field (B_{app}) versus the measured field at the centre of the top surface of the sample (B(Hall)). The simulation results show excellent agreement with the experimental calibration of the applied field as carried out in Hirano *et al* [20]. This validates the modelling framework with respect to the magnetising fixture and its interaction with the sample with the MgB$_2$ in its normal state ($T > T_c$). Reproduced by permission of IOP Publishing from [20].

Figure 6 illustrates the temporal dependence of the applied magnetic field in the simulations, compared to the experiment. Figure 7 meanwhile illustrates the relationship between the applied magnetic field B_{app}, to the measured magnetic field at the Hall probe, B(Hall). In both figures, we observe excellent agreement between the simulation and experimental results. It should be noted the pulse calibration in figures 6 and 7 was
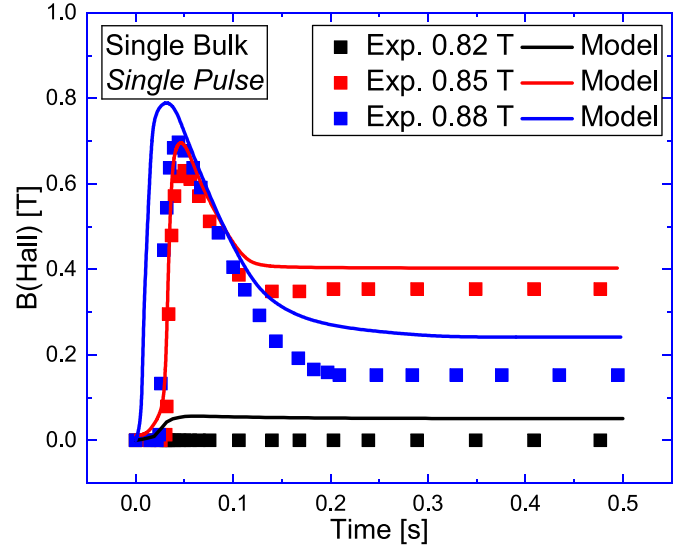

Figure 8. Modelled trapped field (B(Hall)) at the centre of the top surface of the sample ($+0.5$ mm) versus time for the single bulk configuration compared to the experimental data (see figure 2) for applied fields of 0.82, 0.85 and 0.88 T at 20 K. Reproduced by permission of IOP Publishing from [20].

carried out at 40 K with the MgB$_2$ sample in the normal state above its critical temperature T_c, for both the simulation and the experiment.

3.2. Single pulse replication

Next, following the experimental procedure outlined by Hirano *et al* [20], we apply single pulses of varying magnitude to the three sample configurations at 20 K. These are the 'single bulk' without copper layers or inserted iron yoke, the 'composite' bulk with the copper layers and the 'composite with yoke' bulk, with the copper layers and inserted iron yoke (see figure 2). Figure 8 shows the simulation results for the 'single bulk' without copper layers and the iron yoke, for applied fields of 0.82, 0.85 and 0.88 T. There is good qualitative agreement between the simulation and experimental results and reasonable quantitative agreement, with the model slightly over-predicting the trapped field for all applied fields. Figure 9 meanwhile illustrates the replication of the trapped fields for the 'composite without yoke'. The fitting here is likely improved through the addition of the copper layers, which were modelled to have a higher thermal contact conductance between the sample and the sample holder compared to that of the MgB$_2$, as outlined in the thermal assumptions section. This can also be said for figure 10, which illustrates the modelled trapped fields of the 'composite with yoke' configuration. The yoke was modelled with a fixed electrical conductance of 5×10^7 S m^{-1}, and no thermal contact between the sample and the yoke. Whilst estimations were made for the thermal contact conductance between the MgB$_2$ and the sample holder, reference data [38] was used for the conductance between the copper and the sample holder. This is a possible reason for the improved agreement between simulated
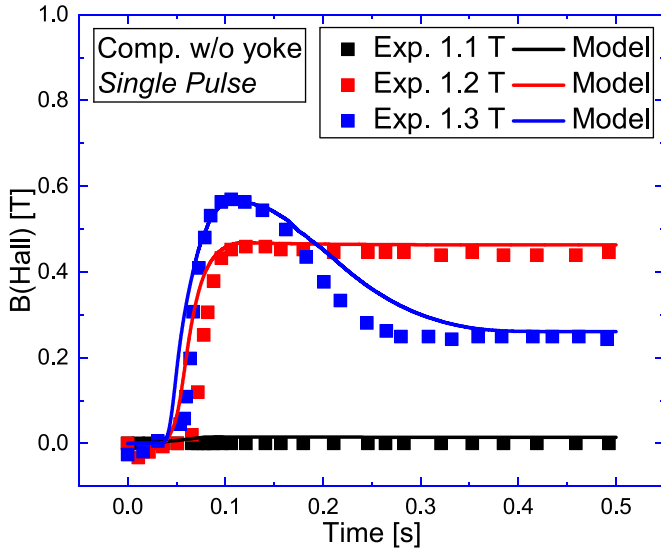
Figure 9. Modelled trapped field (B(Hall)) at the centre of the top surface of the sample (+0.5 mm) versus time for the 'composite without yoke' configuration compared to the experimental data, (see figure 2) for applied fields of 1.1, 1.2 and 1.3 T at 20 K. Reproduced by permission of IOP Publishing from [20].
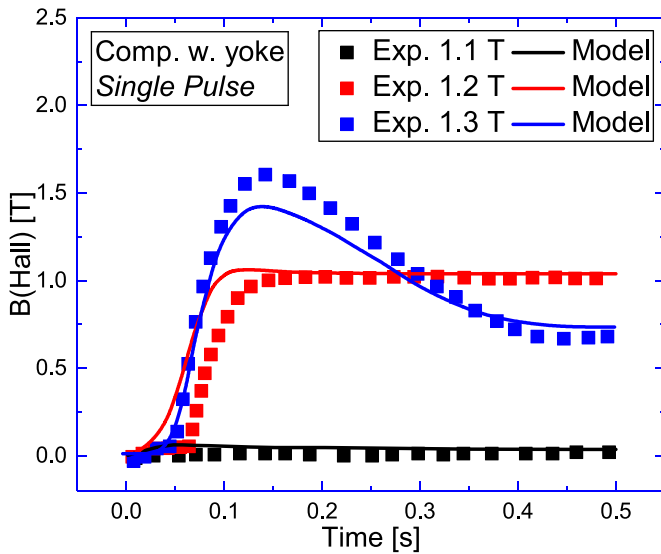

Figure 11. Simulated and experimental results for the maximum temperature recorded at the temperature probe ($r = 48$ mm, $z = 0$) for all sample configurations with varying applied pulse magnitudes. Reproduced by permission of IOP Publishing from [20].

Figure 10. Modelled trapped field (B(Hall)) at the centre of the top surface of the sample (+0.5 mm) versus time for the 'composite with yoke' configuration compared to the experimental data, (see figure 2) for applied fields of 1.1, 1.2 and 1.3 T at 20 K. Reproduced by permission of IOP Publishing from [20].

and experimental results; as the trapped field was observed to be sensitive to this parameter.

Figure 11 illustrates the maximum temperature ($T_{\max}$) recorded at the temperature probe, located at $r = 48$ mm and $z = 0$, embedded within the sample holder. The model represents an axisymmetric construct with an annular sample holder and heat flow is isotropic along the radius. This is not the same as in the experiment as heat flow was anisotropic towards the cold-stage, with the probe on the adjacent side. This may be why the modelled temperature rises were marginally higher
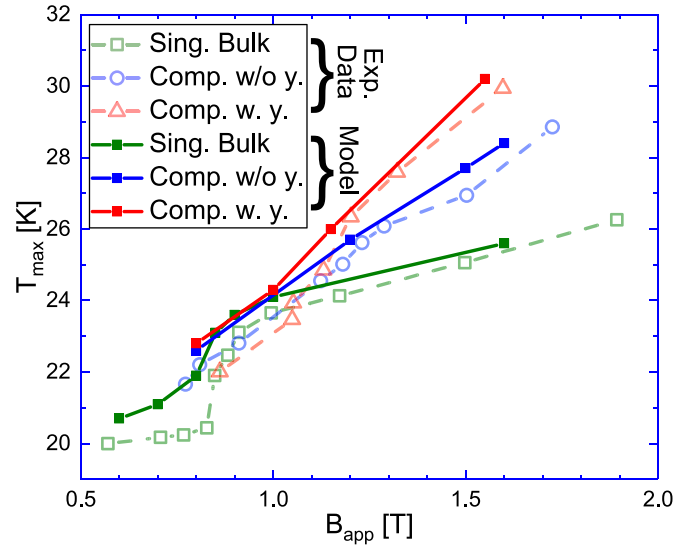
despite well agreed field distributions. It is clear that despite well agreed temperature probe measurements between the simulated and experimental data, the simulated temperature surface plots within figure 12 suggest large temperature differences within the sample may exist. It is not practical to measure the interior of the sample during a pulse, and these modelled plots give insight where the experiment cannot.

The model helps illustrate how the results of Hirano *et al* were achieved. Through the addition of the copper plates the applied pulse was elongated temporally as shown in figure 6, due to the action of Lenz's law on the copper. The modelled thermal contact between these copper slides and the sample holder also permitted the free conduction of heat energy post-pulse, which can be readily interpreted from figure 12. This better cooling may have helped reduce the effect of heating on the pinning forces, which would normally reduce their magnitude. The modelled results were heavily dominated by the flow of heat energy and the sample temperature, for which figure 12 provides interesting insight. Whilst the probe data, which measures the temperature of the sample indirectly via the sample holder, shows good agreement; the temperature within the bulk is significantly higher. It is interesting to further see that despite being both applied with 1.2 T pulses, the 'composite with yoke' arrangement had a significantly higher temperature than the 'composite without yoke'. This is likely due to the larger motion of flux associated with the inserted magnetic yoke. The copper slides are seen as dominant outlets for the flow of heat into the sample holder, illustrating their importance in cooling the bulk. Figures 11 and 12 highlight the difficulties of measuring the temperature directly, but also the utility and insight that numerical can provide to understand the thermal behaviour. The addition of the iron yoke also provided benefit to trapping fields within the bulk. This is due to the assistance the yoke provides in concentrating flux in the
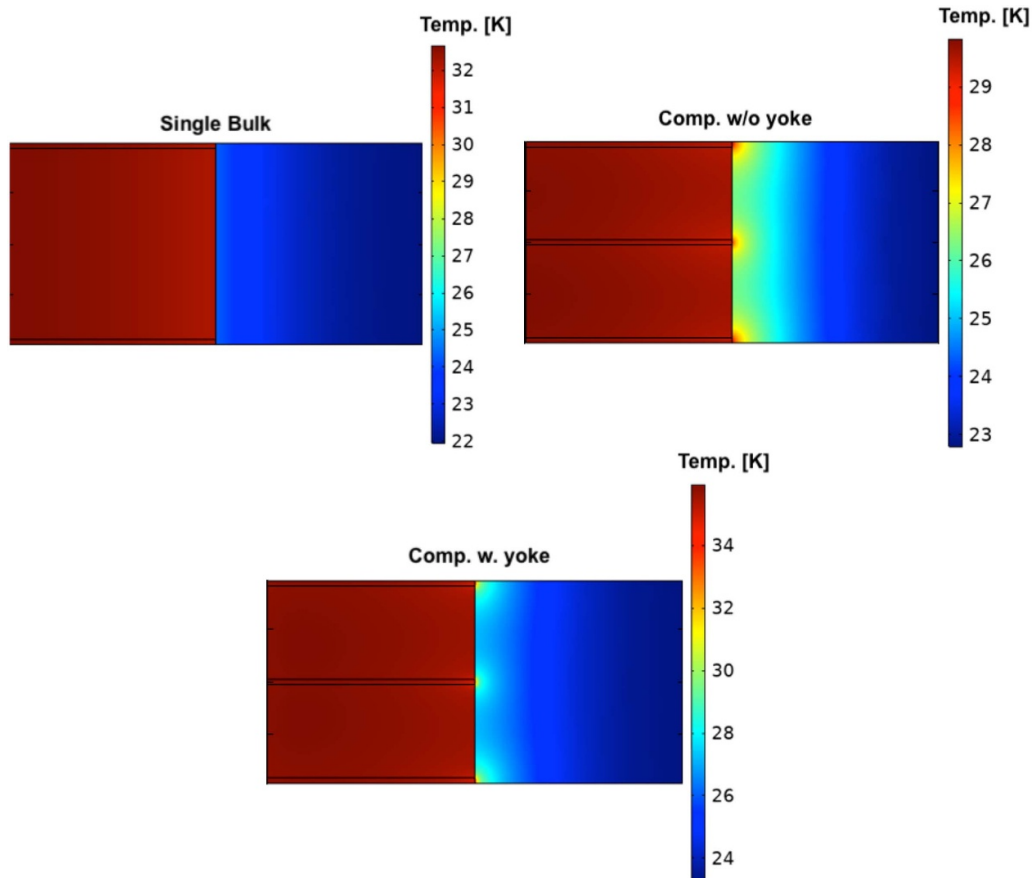
Figure 12. Snapshot of the temperature distribution at 0.5 s for each sample configuration. The bulks, in the order presented, were were subjected to applied pulsed fields of 0.85, 1.2 and 1.2 T, respectively. The probe maximum temperature in the sample holder clearly differs from that within the bulk itself.

bore of the bulk during the pulse. The magnetisation of the iron yoke is weakly temperature dependent below 100 K, meaning it can remain readily magnetised throughout the pulsing. The magnetising currents of MgB_2 meanwhile are strongly temperature (and indeed field) dependent, below 40 K. This fact may be beneficial to future experimentation aiming to trap greater fields, and as we explore later in this paper in the extension studies.

3.3. Double pulse replication

Hirano *et al* [20] also applied a multi-pulse (double-pulse) technique to the bulks, namely to the 'composite with yoke' configuration. This pulsing sequence involved applying two distinct pulses with a large relaxation time between the pulses, and is described in detail in the literature [39]. Applying this method to their samples, Hirano *et al* [20] achieved the record trapped field of 1.61 T. It has been shown by a number of researchers that this technique can lead to an increased trapped field, however there are a larger number of parameters—including the number of pulses, the temperature(s), and pre-magnetised state of the bulk at which they are applied—which need careful optimisation to achieve this [39–43]. Through the application of the first pulse (of magnitude 1.3 T), a uniform

pre-magnetised state of 0.6 T at the centre of the top surface of the sample (+0.5 mm) was achieved. The secondary applied pulses (of magnitude 1.15 T, 1.25 T and 1.5 T) then produced the modelled trapped field represented in figure 13. There is excellent agreement between the experimental data and the modelled results, which were produced without any modification to the simulation assumptions and physics from the single pulse framework. Despite the slight reduction in shielding observed on the 1.15 T pulse, this gives a high level of confidence in the utilisation of these models to carry out the extension studies presented in the following section; which in turn explore the physics of this experiment and attempt to illustrate the primary influencing factors of this complex setup.

4. Extension studies

Above, we have established with carefully-considered numerical models that it is possible to accurately replicate the experimental data of Hirano *et al* [20]. We have accurately replicated the electromagnetic and thermal behaviour, with all three configurations, for the single and multi-pulse cases. Here, we extend this study by investigating the influence of the copper layers and the yoke in magnetising the bulks more effectively.
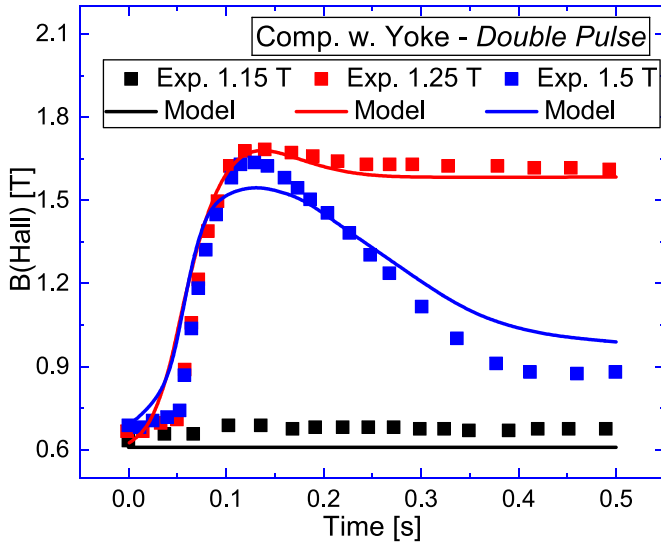
Figure 13. Modelled trapped field (B(Hall)) at the centre of the top surface of the sample versus time for the 'composite with yoke' configuration under the double-pulse sequence as outlined in [20], compared to the experimental data, for applied fields of 1.15, 1.25 and 1.5 T at 20 K. Reproduced by permission of IOP Publishing from [20].

Figure 14. Modelled applied field (B(Hall)) at the centre of the top surface of the sample versus time for the 'composite without yoke' configuration at 40 K. We modify the number of copper layers (N) in the bulk from three up to ten, spacing them equidistantly.

4.1. Influence of copper layer number

In the experiment presented by Hirano *et al* [20], three copper layers were inserted into two of the bulk configurations. These layers were added to elongate the applied pulse, through the induction of eddy-currents in the copper. Hence for each added copper layer, the rise-time of the applied pulse can be extended; but simultaneously the volume of superconductor is reduced. To quantify this effect and determine the optimum number of copper layers, we vary the number of layers, N, from three to ten, spaced equidistantly throughout the sample. Figure 14 illustrates the modelled field at the centre of the top surface of these samples at 40 K, with an applied field (B_{app}) of 1.03 T. This pulse has the same magnitude and rise-time used by Hirano *et al* in their 40 K calibration tests (figure 5(a) in [20]). In figure 14, the applied pulse (black line) is compared to the modelled pulses for varying layer number (coloured). It can be seen that the applied pulse rise time (t_{rs}) is elongated to 70 ms, and the magnitude reduces to approximately 0.78 T for the three-layer configuration, showing good agreement with the experimental data (as seen in figure 6). Comparing the case for layer number $N = 3$, and $N = 10$, we can see that the applied field magnitude and rise time changes by a further -0.34 T and 75 ms, respectively. The maximum temperature recorded for the $N = 3$ and $N = 10$ cases was 40.99 K and 40.83 K respectively, compared to that of 40.63 K for the no layer case. The difference in temperature rises are small, as the specific heat of copper is over eight times larger at 40 K than at 20 K. Whilst the applied pulse magnitude (B_{app}) remains constant, the field at the Hall probe (B(Hall)) decreases with each additional layer. Hence, the small decrease in temperature with additional layers indicates that increasing the number of copper layers does not significantly reduce the sample heating.
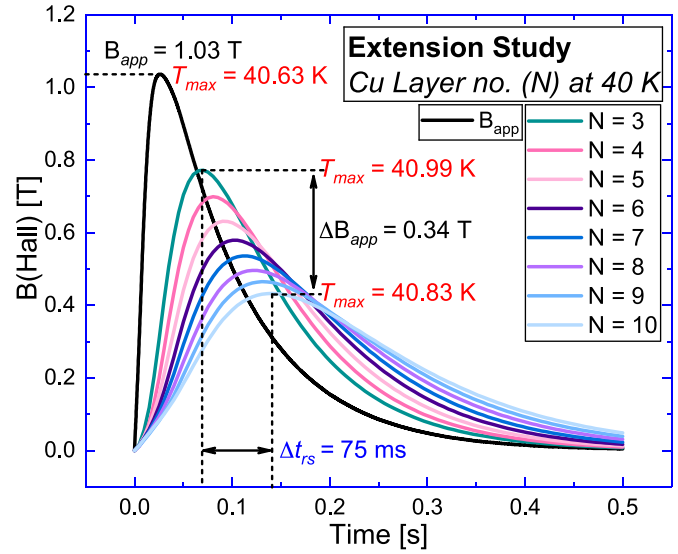
Despite this negligible change in temperature, the increased shielding and pulse retardation of more layers is not negligible. This result indicates that larger, more expensive magnetising equipment would be required to access higher trapped fields for samples with many copper layers. Further, elongating the pulse reduces the applied field magnitude. Therefore, to apply a field of similar magnitude, a higher capacitor bank voltage (and hence stored energy) is required. Given the increased heating at larger field magnitudes, it seems the choice of three layers by Hirano *et al* was a considerably appropriate one.

The ambient temperature of 40 K was chosen to eliminate the influence of the MgB_2 supercurrent, and investigate the interaction of the copper layers only with the applied field. Now, in figure 15, we have modelled the 'composite without yoke' sample at 20 K to investigate the trapped field potential of the samples when superconducting. Single pulses of magnitude 1.03 T and 2.00 T were applied to samples with copper layer numbers between $N = 2$, and $N = 10$. The additional layer of $N = 2$ was chosen here to capture the peak at the lower applied field. These two pulse magnitudes were chosen to illustrate how larger fields are required to effectively penetrate samples with higher layer numbers. The magnetic field plotted (B_{trap}(centre)) was calculated in the simulation at the centre of the sample bore ($r = 0$, $z = 0$), in contrast to B(Hall) measured in the location of the Hall probe. This was chosen to make a better comparison to the sample shielding and penetration. We define the sample penetration as the displacement along the cut line $z = 0$ from the outer sample radius to the inner radius, that has not shielded the applied pulse. For example, 70% penetration would mean the bulk shielded the pulse up to $r = 16$ mm (14 mm past the outer radius) along the $z = 0$ line. For the 1.03 T pulses, the peak trapped field occurred for $N = 2$ layers. For higher layer numbers, 'M-shaped' magnetisation profiles were observed with sample penetration dropping from 98% of
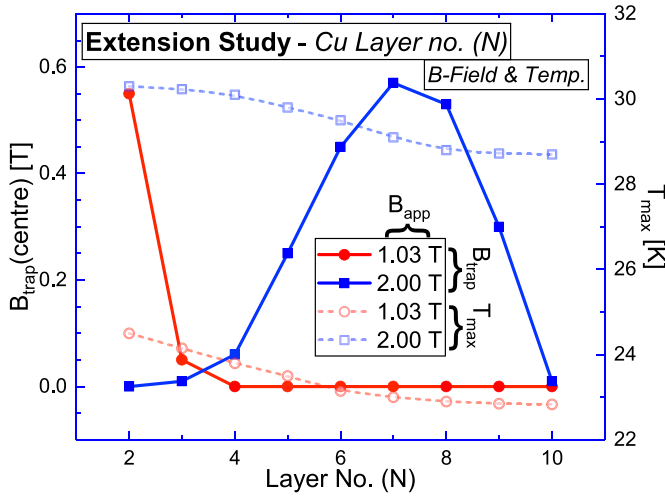
Figure 15. Modelled trapped field (B_{trap}(centre)) at the centre of the sample bore ($r = 0$, $z = 0$) for the 'composite without yoke' configuration at 20 K. The number of copper layers (N) in the bulk is modified from two up to ten, spacing them equidistant. On the right y-axis is the maximum temperature rise for each layer number and pulse.

Figure 16. Modelled trapped field (B_{trap}) at the centre of the top surface of the 'composite without yoke' with applied field (B(shunt)), for varying copper layer number (N). The maximum trapped field is observed for the case of five copper layers. Reproduced by permission of IOP Publishing from [20].

the radius for $N = 3$, to just 30% for $N = 10$. The 'single bulk' ($N = 0$) trapped negligible or zero field for both pulse magnitudes. The peak trapped field for the 2.00 T pulses occurs for $N = 7$, trapping 0.58 T. Sample penetration was 100% for all layer numbers up to $N = 10$, where it drops to 95%. For the 2.00 T pulse, with layer numbers $N < 7$, the sample could not trap the large applied field and was heated above 27 K. For layer numbers $N \geqslant 7$, the added layers increased the rise-time and reduced the pulse magnitude, resulting in reduced heating. The maximum temperature profiles illustrate how both pulses are moderated by the presence of the layers, with diminishing effect towards the highest layer numbers. Knowing from figure 14 that the applied pulse for $N = 10$ is much lower in magnitude and greater in rise time, helps explain these smaller temperature increases. It is clear from figure 15 that whilst larger pulses are required to access and effectively trap uniform fields at the centre of the bulk, the increased heating limits the trapped field performance of the bulk. This means that whilst the thermal performance of samples with a higher layer number is improved, it is not enough to abate the heating of the large pulses required to trap a field effectively in the MgB$_2$.

Finally, in figure 16 we investigate how varying the magnitude of the applied field to the composite bulks affects the trapped field at the centre of the top surface of the bulk, with increasing layer number. This should elucidate the optimum number of layers to trap the maximum field in the sample. There is good agreement between the experimental data and the model for the case of three layers. Increasing the layer number at first increases trapped field performance, but at the cost of needing to apply higher fields. For the case of $N = 5$ layers, a maximum trapped field of 0.65 T was observed at 1.6 T applied field. As layer number increases, the volume of superconducting material decreases, and the subsequent trapped field performance reduces above five layers. This
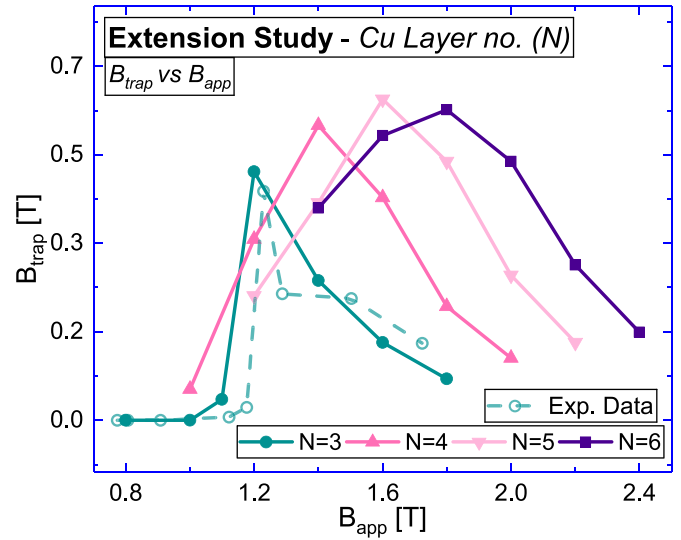
again indicates that the use of three copper layers was a considerably appropriate choice by Hirano *et al* [20], when considering an increment of 0.4 T in applied field yields an additional trapped field of less than 0.2 T for the $N = 5$ case.

4.2. Influence of iron yoke insertion

The three sample configurations investigated by Hirano *et al* [20] were progressively augmented, to first include copper plates and then also an iron yoke. As a result, the iron yoke was investigated only with the addition of copper plates. Below, we present a study investigating the case of a 'single bulk *with* iron yoke', to investigate the effect of the iron yoke in magnetising the 'single bulk', with the absence of copper plates.

First, we examine how the iron yoke modulates the applied pulse in the absence of copper layers. Figure 17 illustrates how an applied pulse of 1.03 T is enhanced by the soft-iron yoke at 40 K. The dashed black line shows an applied pulse (B_{app}) of 1.03 T, and the dashed red line (B(Hall)) of the simulated pulse at the centre of the top surface of the yoke. The pulse rise-time is increased slightly due to the finite conductivity of the iron yoke, whilst the magnitude is enhanced significantly due to its ferromagnetic properties. Despite this large enhancement of the magnetic field, the maximum temperature of the bulk was 40.8 K when in the normal state, in part due to assuming no thermal contact between the iron yoke and bulk. The effect of the iron yoke contrasts significantly to the copper layers, which reduce the applied field magnitude and extend the pulse rise time more significantly. This also reduces the requirement from the viewpoint of the magnetising fixture with a composite iron yoke bulk, due to the enhancing effect of the yoke on the applied field from 1.03 T to 2.2 T. Figure 17 also illustrates how three different pulses (of magnitude 0.7 T to 0.8 T) affect the trapped field of the bulk at 20 K. With an applied field
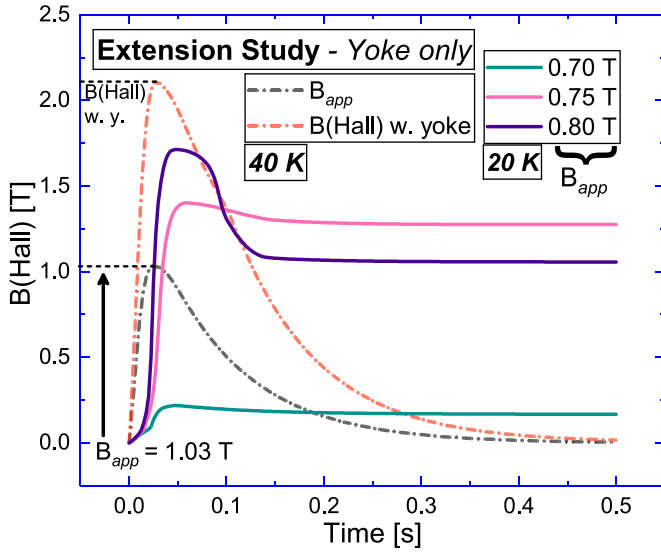
Figure 17. Modelled field (B(Hall)) at the centre of the top surface of the sample versus time for the 'single bulk with yoke' configuration at both 20 K and 40 K. The pulses at 40 K illustrate how the iron yoke enhances the applied pulse, and those at 20 K illustrate the trapped field behaviour.
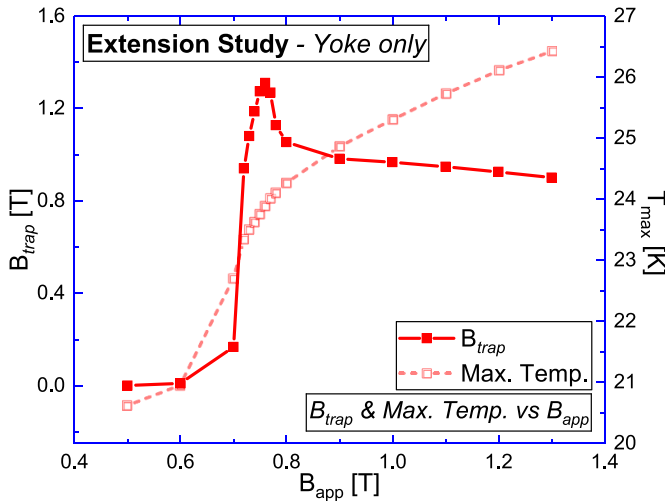

Figure 19. Modelled trapped field (B_{trap}) distribution along the top surface of the bulk +0.5 mm, for the 'single bulk with yoke' configuration. A shift in the contribution of magnetisation between the iron yoke and MgB$_2$ can be observed with increasing applied pulse magnitude (B_{app}).

Figure 18. Modelled trapped field (B_{trap}) at the centre of the top surface of the sample for the 'single bulk with yoke' configuration and maximum temperature (at the temperature probe) with increasing applied pulse magnitude (B_{app}). A rapid increase in temperature is observed around the peak trapped field.

of 0.7 T, the bulk has mostly shielded the applied field, trapping only 0.17 T. The peak trapped field for this bulk occurs for the applied field of 0.75 T, trapping 1.27 T due to the flux concentrating properties of the iron yoke. At higher applied fields however, the trapped field begins to decrease. This effect can be better explained with reference to figure 18, discussed below.

Figure 18 illustrates the trapped field performance (B_{trap}) and maximum temperature (T_{max}) of the bulk, against applied field magnitude (B_{app}). A sharp peak in trapped field is observed at 0.75 T applied field, tending towards a trapped field of approximately 1.0 T at larger applied fields. A rapid
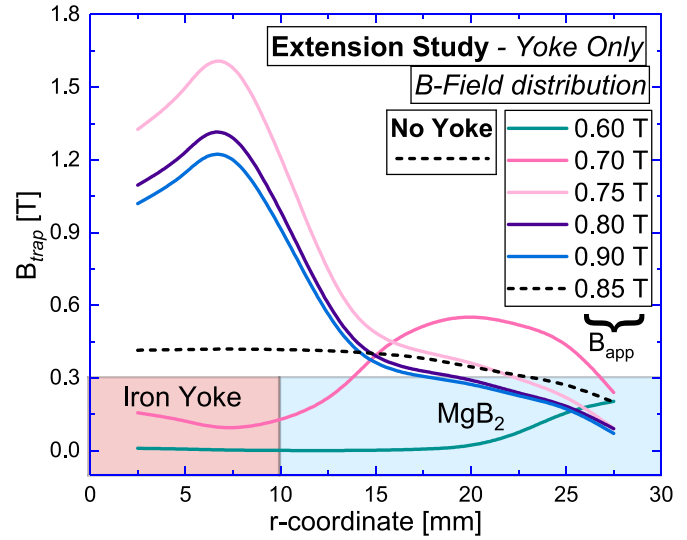
rise in the maximum temperature is simultaneously observed around this peak, followed by a reduced rate of temperature increase at larger applied fields. This behaviour is observed in the 'single bulk' case of figure 11 with a lower temperature rise compared to the 'yoke only' case. It appears that the flux concentrating properties of the iron yoke assists in retaining the magnetisation of the entire bulk, despite the significant heating. The heating rate is reduced once the composite bulk (i.e. 'single bulk' with iron insert) magnetisation 'saturates' past $B_{\text{app}} = 0.8$ T, which is evident from the two distinct gradients in the slope of T_{max}. Compared to the 'single bulk' case, the applied field which yields the peak trapped field is reduced from 0.85 T to 0.75 T when inserted with the iron yoke. The stronger performance of the 'single bulk with yoke' sample at higher applied fields compared to the 'single bulk' can be attributed to the addition of the soft-iron yoke.

Figure 19 illustrates how the magnetic field is trapped within the 'single bulk with yoke' composite, in response to the applied pulses. The field was sampled at ten points along the top surface of the bulk +0.5 mm, every 2.5 mm in a style similar to a Hall array. The point of 10 mm was not sampled due to a saturating effect on the B-field distribution caused by the sharp corner of the yoke. With an applied pulse of 0.6 T, the bulk has mostly shielded the applied field. With increasing magnitude however, the bulk begins to trap greater fields. At 0.7 T applied field, the MgB$_2$ magnetisation peaks with an M-shaped distribution, and some magnetisation of the iron yoke. At applied fields of 0.75 T and greater, the iron yoke contributes the greatest magnetisation of the sample, whilst at lower applied fields, the MgB$_2$ itself contributes greater magnetisation. The peak in magnetic field towards the edge of the iron yoke at 10 mm is caused by the sharp geometry/corner of the yoke. The field was not sampled at 10 mm in figure 19 to remove this saturating effect on the figure. Despite forming a

less uniform field than a disc-shaped bulk, this bulk composite has enhanced the trapped field at the centre of the bulk. The iron yoke and MgB_2 components of the bulk work collaboratively to enhance the magnetisation of the bulk, and retain greater and more consistent fields when pulsed at higher magnitudes. This could be useful for other composite bulk arrangements that operate over a larger temperature and field range, such as the hybrid trapped field magnet lens developed by Takahashi, Fujishiro and Ainslie [44–46].

5. Conclusions

We have demonstrated that the reported data of Hirano *et al* [20] can be replicated with an accurate FEM modelling framework, whereby a trapped field record in an MgB_2 composite bulk using PFM was achieved. With careful calibration of the modelled physics and geometry, we have validated the modelling framework against the measured FCM performance of the bulk. Further, the experimental PFM data is validated for both single- and multi-pulse regimes, for three sample configurations: the 'composite with yoke' with copper layers and inserted iron yoke, the 'composite' with copper layers (no yoke), and the 'single bulk' ring (without either copper layers or inserted yoke). Importantly, we successfully modelled the trapped field record of 1.61 T via PFM using a multi-pulse technique, with excellent quantitative agreement. Using these models we have gained insight into the physics and mechanisms that produced the experimental results, and explained how the transit of heat influenced the results obtained. We found that decreasing the contact conductance between the MgB_2 bulk and the sample holder at higher temperatures improved the accuracy of the models, and speculate a physical explanation for this with the help of figure 4.

The models are then extended to investigate the effect of trapped field with a change in the number of copper layers, which indicated this configuration achieved maximum trapped field at $N = 5$ layers for $B_{app} = 1.6$ T. However, this finding indicates an additional burden on the magnetisation fixture, where a higher applied pulse current is required to effectively magnetise samples with a higher number of copper layers. It is shown how the number of copper layers impacts both the elongation of the applied pulsed field and its magnitude, and how this affects the trapped field in the composite bulk. We have also illustrated that the copper layers influence the thermodynamic behaviour of the composite bulk. We found that increasing the number of copper layers reduces the maximum temperature rise of the bulk, due to reduced magnetic field penetration and the additional high thermal conductance pathways created by these layers for cooling the bulk during pulsing. We conclude that a choice of three layers was a suitable compromise between the benefits and drawbacks of the copper layers.

Finally, the influence of the iron yoke inserted into the composite bulk was investigated in detail, which was not reported in the original experiments. The soft-iron yoke inserted into the 'single bulk' configuration increases the effective magnitude of the applied pulse, and acts to concentrate flux during the pulse and retain it after the pulse, even for high applied fields that would normally result in significantly lower trapped fields without the presence of the yoke. The enhancing magnetising effect of the soft-iron yoke may allow for more compact and efficient magnetising coil design, using smaller coils and lower applied fields.

These results will help guide further experimentation allowing researchers to determine how these complex parameters may influence the optimal trapped field and produce better bulk superconducting magnets.

Data availability statement

The data that support the findings of this study are openly available at the following URL/DOI: https://doi.org/10.17863/CAM.69446.

ORCID iDs

V Cientanni ⃝ https://orcid.org/0000-0001-6621-2733
M D Ainslie ⃝ https://orcid.org/0000-0003-0466-3680
H Fujishiro ⃝ https://orcid.org/0000-0003-1483-835X
K Takahashi ⃝ https://orcid.org/0000-0002-8278-2688

References

[1] Hull J R and Murakami M 2004 *Proc. IEEE* **92** 1705–18
[2] Watson J and Younas I 1998 *Mater. Sci. Eng.* B **53** 220–4
[3] Nagaya S, Kashima N, Minami M, Kawashima H and Unisuga S 2001 *IEEE Trans. Appl. Supercond.* **11** 1649–52
[4] Song J, Choi Y, Yang D, Kim Y, Kim K and Lee H 2017 *Results Phys.* **7** 3264–76
[5] Durrell J H *et al* 2014 *Supercond. Sci. Technol.* **27** 082001
[6] Kambara M, Babu N H, Sadki E S, Cooper J R, Minami H, Cardwell D A, Campbell A M and Inoue I H 2001 *Supercond. Sci. Technol.* **14** L5–7
[7] Durrell J H *et al* 2012 *Supercond. Sci. Technol.* **25** 112002
[8] Naito T, Takahashi Y and Awaji S 2020 *Supercond. Sci. Technol.* **33** 125004
[9] Fuchs G, Häßler W, Nenkov K, Scheiter J, Perner O, Handstein A, Kanai T, Schultz L and Holzapfel B 2013 *Supercond. Sci. Technol.* **26** 122002
[10] Bhagurkar A G, Yamamoto A, Wang L, Xia M, Dennis A R, Durrell J H, Aljohani T A, Babu N H and Cardwell D A 2018 *Sci. Rep.* **8** 13320
[11] Sugino S, Yamamoto A, ichi Shimoyama J and Kishio K 2015 *Supercond. Sci. Technol.* **28** 055016
[12] Krabbes G, Fuchs G, Canders W R, May H and Palka R 2006 *High Temperature Superconductor Bulk Materials Fundamentals, Processing, Properties Control, Application Aspects* (Germany: Wiley-VCH)

[13] Fujishiro H, Hiyama T, Miura T, Naito T, Nariki S, Sakai N and Hirabayashi I 2009 *IEEE Trans. Appl. Supercond.* **19** 3545–8

[14] Mizutani U, Oka T, Itoh Y, Yanagi Y, Yoshikawa M and Ikuta H 1998 *Appl. Supercond.* **6** 235–46

[15] Ainslie M D, Fujishiro H, Ujiie T, Zou J, Dennis A R, Shi Y H and Cardwell D A 2014 *Supercond. Sci. Technol.* **27** 065008

[16] Patel A, Hopkins S C and Glowacki B A 2013 *Supercond. Sci. Technol.* **26** 032001

[17] Fujishiro H and Naito T 2010 *Supercond. Sci. Technol.* **23** 105021

[18] Wu H, Yong H and Zhou Y 2018 *Supercond. Sci. Technol.* **31** 045008

[19] Fujishiro H, Mochizuki H, Naito T, Ainslie M D and Giunchi G 2016 *Supercond. Sci. Technol.* **29** 034006

[20] Hirano T, Takahashi Y, Namba S, Naito T and Fujishiro H 2020 *Supercond. Sci. Technol.* **33** 085002

[21] Ida T, Shigeuchi K, Okuda S, Watasaki M and Izumi M 2016 *J. Phys.: Conf. Ser.* **695** 012009

[22] Ida T, Li Z, Miki M, Watasaki M and Izumi M 2018 *IEEE Trans. Appl. Supercond.* **28** 1–5

[23] Ainslie M D and Fujishiro H 2015 *Supercond. Sci. Technol.* **28** 053002

[24] Ainslie M D and Fujishiro H 2019 *Numerical Modelling of Bulk Superconductor Magnetisation* (Bristol: IOP Publishing) pp 1–18

[25] Ainslie M D *et al* 2016 *Supercond. Sci. Technol.* **29** 074003

[26] Takahashi K, Ainslie M D, Fujishiro H, Naito T, Shi Y H and Cardwell D 2017 *Physica* C **536** 1–10

[27] Fujishiro H, Mochizuki H, Ainslie M D and Naito T 2016 *Supercond. Sci. Technol.* **29** 084001

[28] Ogino A, Naito T and Fujishiro H 2017 *IEEE Trans. Appl. Supercond.* **27** 1–5

[29] Naito T, Ogino A and Fujishiro H 2016 *Supercond. Sci. Technol.* **29** 115003

[30] Neumeier J J, Tomita T, Debessai M, Schilling J S, Barnes P W, Hinks D G and Jorgensen J D 2005 *Phys. Rev.* B **72** 220505

[31] Simmons R O and Balluffi R W 1957 *Phys. Rev.* **108** 278–80

[32] Cavallin T, Young E A, Beduz C, Yang Y and Giunchi G 2007 *IEEE Trans. Appl. Supercond.* **17** 2770–3

[33] Wang Y, Plackowski T and Junod A 2001 *Physica* C **355** 179–93

[34] Simon N J, Drexler S and Reed R P 1992 7 *Properties of Copper and Copper Alloys at Cryogenic Temperature* vol 177 (Gaithersburg, MD: National Institute of Standards and Technology CY) pp 1–16

[35] Guillet A and Delamarre F 2015 Condensed matter (arXiv:1503.01279)

[36] Kemp W, Klemens P and White G 1956 *Aust. J. Phys.* **9** 180–8

[37] Zhang K, Ainslie M, Calvi M, Hellmann S, Kinjo R and Schmidt T 2020 *Supercond. Sci. Technol.* **33** 114007

[38] Choi Y S and Kim M S 2014 *AIP Conf. Proc.* **1573** 1070–7

[39] Fujishiro H, Tateiwa T, Fujiwara A, Oka T and Hayashi H 2006 *Physica* C **445–8** 334–8 *Proceedings of the 18th Int. Symp. on Superconductivity (ISS 2005)*

[40] Kamijo H and Fujimoto H 2001 *IEEE Trans. Appl. Supercond.* **11** 1816–19

[41] Sander M, Sutter U, Koch R and Kläser M 2000 *Supercond. Sci. Technol.* **13** 841–5

[42] Yanagi Y, Itoh Y, Yoshikawa M, Oka T, Ikuta H and Mizutani U 2005 *Supercond. Sci. Technol.* **18** 839–49

[43] Ainslie M D, Srpcic J, Zhou D, Fujishiro H, Takahashi K, Cardwell D A and Durrell J H 2018 *IEEE Trans. Appl. Supercond.* **28** 1–7

[44] Takahashi K, Fujishiro H and Ainslie M D 2018 *Supercond. Sci. Technol.* **31** 044005

[45] Takahashi K, Fujishiro H, Namba S and Ainslie M D 2021 *Supercond. Sci. Technol.* **34** 05LT02

[46] Namba S, Fujishiro H, Naito T, Ainslie M D and Takahashi K 2019 *Supercond. Sci. Technol.* **32** 12LT03